eScience xxx (xxxx) xxx

Contents lists available at ScienceDirect

eScience

journal homepage: www.keaipublishing.com/en/journals/escience

Polypyrrole as an ultrafast organic cathode for dual-ion batteries

Tao Sun [a,1], Qi-Qi Sun [a,b,1], Yue Yu [a], Xin-Bo Zhang [a,*]

[a] State Key Laboratory of Rare Earth Resource Utilization, Changchun Institute of Applied Chemistry, Chinese Academy of Sciences, Changchun, 130022, PR China
[b] National & Local United Engineering Laboratory for Power Batteries, Faculty of Chemistry, Northeast Normal University, Changchun, Jilin, 130024, PR China

ARTICLE INFO

Keywords:
Polypyrrole
Organic electrode
Conductive polymers
Dual-ion batteries

ABSTRACT

Organic electrode materials based on the chemical bond cleavage/recombination working principle usually produce unimpressive reaction kinetics and stability. In this work, polypyrrole (PPy) is investigated as an ultrafast (87% retention at 20 A g^{-1}) and stable (83% retention across 3000 cycles) cathode material in PPy||graphite dual-ion batteries. The fast intrinsic reaction kinetics, coupled with a capacitance-dominated mechanism, enable PPy to bypass the sluggish chemical bond rearrangement process. Electrochemically induced secondary doping improves the ordered aggregation of polymer chains and thus has a profound impact on anion diffusion and electrical conductivity. The excellent rate capability presented here changes our understanding of organic electrode materials and could prove useful for designing ultrafast rechargeable electrochemical devices.

1. Introduction

Energy storage devices such as lithium-ion batteries (LIBs) have profoundly changed modern ways of living [1,2], but in the face of sustainability requirements, extensive research has been devoted to developing alternative battery systems [3–5]. Among these, dual-ion batteries (DIBs) are emerging as promising candidates [6–8]. A prominent example of DIBs is the dual-graphite battery (DGB), which substitutes a transition metal-based cathode with carbon-based materials and thereby is more recyclable and environmentally friendly [9,10]. Unfortunately, the electrolyte in commercial LIBs decomposes when the anion intercalates with graphite at a high potential, so most DGBs rely on ionic liquid electrolytes [11,12]. From an economic standpoint, though, the production cost of batteries will be significantly increased if the current carbonate-based electrolytes are replaced by ionic liquids. Moreover, the high viscosity of an ionic liquid significantly restricts ion transport. It is therefore essential to find suitable cathode materials that will be compatible with the current electrolyte system.

To accommodate bulky anions reversibly, the host structure should possess large interstitial sites. As it happens, an inherent characteristic of organic electrode materials (OEMs) meets this requirement. Assembled by van der Waals forces, OEMs feature large spacing and flexible hosts, making them ideal elastic buffer structures for accommodating the continuous insertion and extraction of anions [13–16]. In the quest to achieve sustainable energy storage devices, the prospect of using OEMs in rechargeable batteries has become increasingly attractive because their components are readily available and their structures can be engineered at the molecular level [17,18]. Yet despite great achievements with OEMs, their application is plagued by problems [19]. Aside from their poor intrinsic electrical conductivity and high solubility in electrolytes, another challenge is their unimpressive rate capability [20].

With the ongoing proliferation of portable electronics and electric vehicles, the demand for high-power-density batteries has become urgent. Although great efforts have been made to improve their rate performance, most of the strategies are focused on optimizing electron and ion transport at the electrode interface or shortening their migration paths [21]. Introducing conductive carbon into organic materials to form composite electrodes offers opportunities to solve the problem of poor electrical conductivity [22]. However, a large amount of conductive carbon is required to ensure sufficient conductivity, which inevitably dilutes the energy density of the whole device. Nanostructuring has been widely employed to increase the rate capability of energy storage materials [20], but the emergence of extrinsic pseudocapacitive electrochemical features is unavoidable with nanoscale electrode materials, so the effect of external assistance is usually limited [23,24].

One fundamental strategy is to prepare an electrode material with intrinsically high reaction kinetics. Taking conjugated carbonyl (C═O) compounds as an example, the working principle of an n-type organic electrode is based on the reversible cleavage/recombination of the C═O bond between the neutral state and the negatively charged state, making

* Corresponding author.
E-mail address: xbzhang@ciac.ac.cn (X.-B. Zhang).
[1] These authors contributed equally to this work.

https://doi.org/10.1016/j.esci.2021.11.003
Received 28 June 2021; Received in revised form 19 October 2021; Accepted 9 November 2021
Available online xxxx

the kinetics intrinsically slow [25]. Since the generation of highly active radical anion intermediates is virtually unavoidable, it is essential to improve the intrinsic electrochemical stability of OEMs. The chemical bond rearrangement process generally demands a relatively high activation energy and is usually accompanied by undesirable side reactions that adversely affect the stability and redox kinetics [18].

In comparison, p-type organic electrodes such as conductive polymers (CPs) usually exhibit fast reaction kinetics [25]. Thanks to charge delocalization in the conjugated structure, the redox center in CPs can achieve stability, thereby avoiding chemical bond rearrangement and enhancing the intrinsic electrochemical stability [26]. Unlike Li^+, which has a large solvation radius because of its strong Lewis acidity, CPs' weak degree of solvation ensures the anions have ready mobility in the electrolyte. Hence, CPs are promising candidates for fabricating ultrafast DIBs.

Among these, polypyrrole (PPy) is especially promising for its reversible doping mechanism, good conductivity, low cost, and facile synthesis [20]. As a typical intrinsic pseudocapacitive material, PPy has a surface redox pseudocapacitive charge storage mechanism, which involves faradaic reactions occurring with charge transfer [26]. Unfortunately, few studies have focused on exploring the potential of PPy in high-rate electrochemical devices.

In this work, ultrafast DIBs were prepared using PPy as the cathode, graphite as the anode, and a common LIB electrolyte (1.0 M $LiPF_6$ in EC/DMC) (Scheme 1). Impressively, these PPy||graphite dual-ion batteries (PGDBs) charged quickly and showed highly stable cycling performance. Surprisingly, their inherent high rate performance was also available with a LiTFSI-based electrolyte and even in a PPy||K battery. To determine the cause of this outstanding rate capability, we conducted fundamental investigations of the electrochemical reaction kinetics, charge transfer at the electrode/electrolyte interface, and ion diffusion dynamics. This work highlights the importance of understanding the intrinsic reaction kinetics of CPs, presenting new angles for preparing high-performance and sustainable energy storage devices.

2. Results and discussion

PPy has been of interest for energy storage applications for decades [20,27]. Its macromolecular structure and doping state are highly sensitive to reaction conditions, which can disrupt the conjugated backbone and thereby affect the polymer's electronic and redox properties. Unlike previous synthesis methods, our process pays particular attention to the feed procedure. The dropwise addition of oxidant permits homogeneous nuclei expansion and full growth of the polymer chain. Sodium *p*-toluenesulfonic acid (*p*TSNa) and $Fe_2(SO_4)_3$ were employed as the anionic dopant and oxidant, respectively (Fig. S1 and Tables S1 and S2). When doping was done with large surfactant anions, the conductivity of PPy reached 14.3 S cm^{-1}, guaranteeing intrinsic electronic conductivity and avoiding the need for a large amount of conductive carbon additive.

As shown in Fig. 1a, the PGDBs displayed sloping charge/discharge curves with a median discharge voltage of 3.1 V at a current of 50 mA g^{-1}. With CP-based electrode materials, the charge/discharge profiles of PGDBs do not exhibit a flat voltage plateau, due to the variable doping level. Compared with a PPy||Li half-cell, the electrochemical characteristics of PPy were well retained in dual-ion full cells (Fig. S2). It is worth noting that a gradual increase in capacity occurred during the initial cycling (Fig. S2). Due to insufficient contact between polymer and electrolyte, the capacity-increasing stage can be identified as an "activation process". Once the polymer surface was sufficiently exposed to the electrolyte, the active site availability and reaction kinetics improved. Compared with bulky *p*-toluenesulfonate (pTS^-) and divalent sulfate, monovalent PF_6^- anions were newcomers. Consequently, there was an adjustment and adaptation process in the initial cycles until a steady, optimal state was reached.

The increase in specific capacity during the activation process was also revealed by cyclic voltammetry (CV), with the area inside the CV

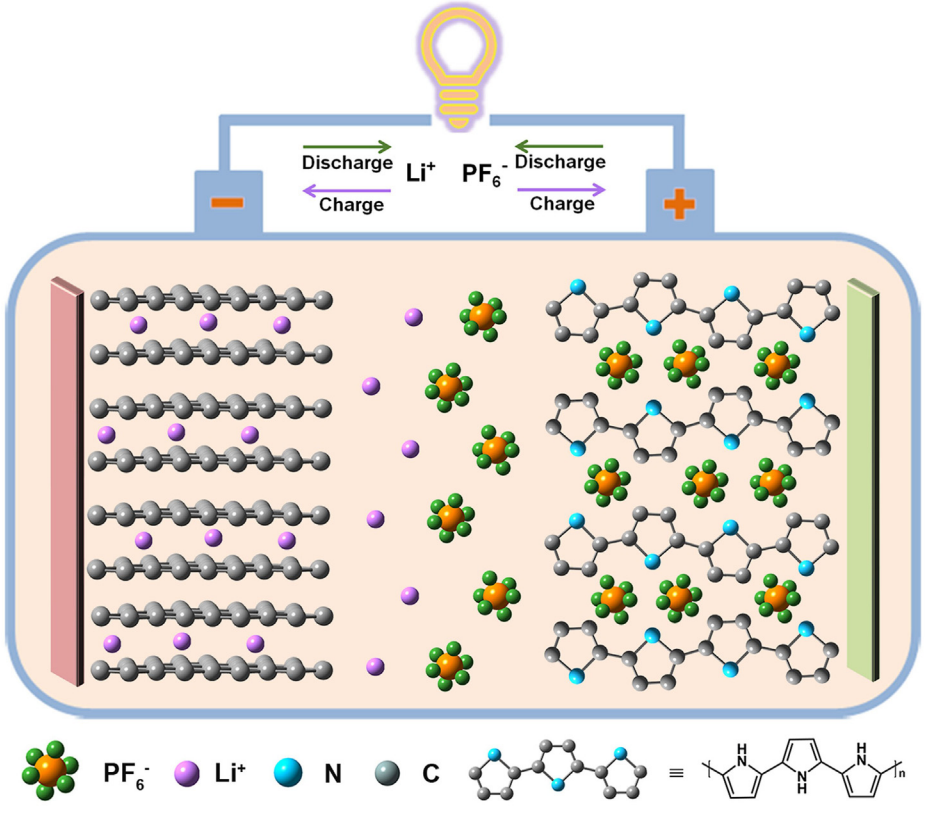

Scheme 1. Schematic representation of PPy||graphite dual-ion batteries.

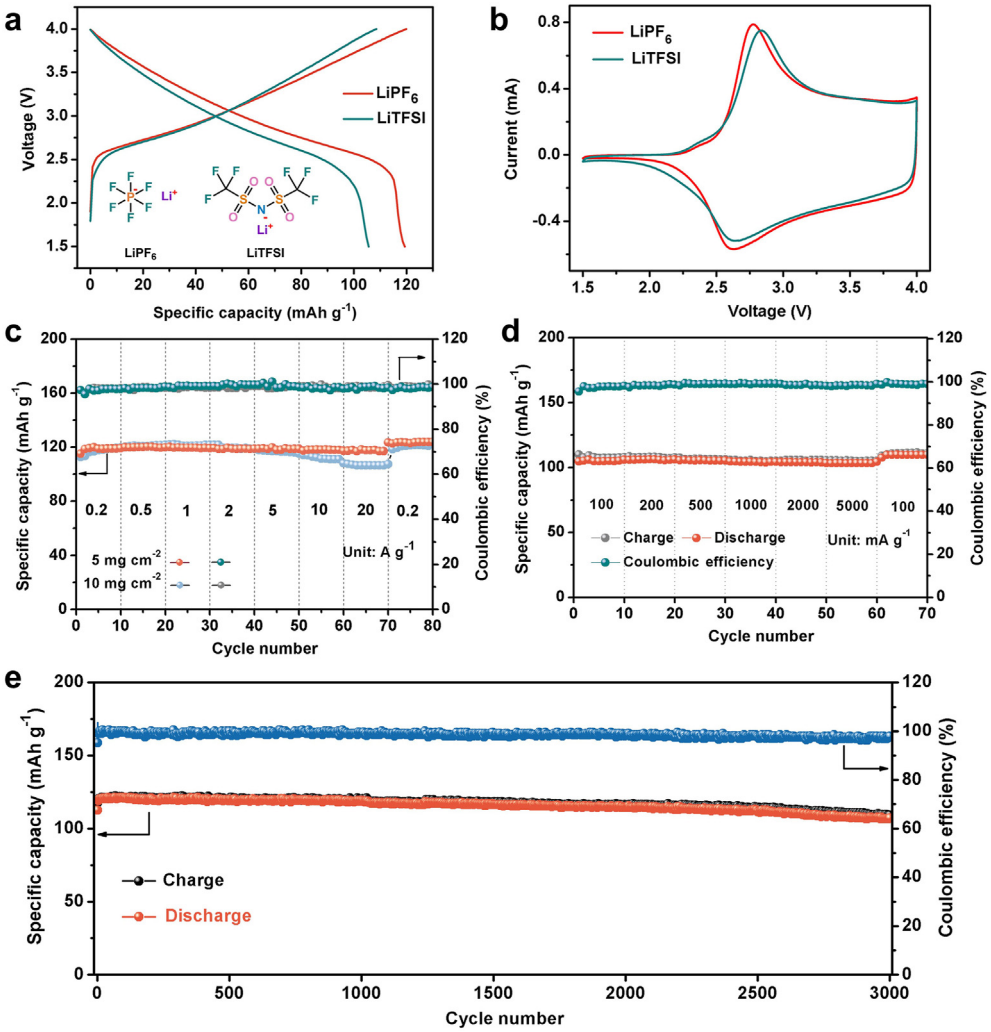

Fig. 1. (a) Discharge/charge profiles of PGDBs at a current of 50 mA g^{-1}. (b) CV curves of PGDBs at a scan rate of 0.2 mV s^{-1}. (c) Rate performance of PGDBs with different mass loadings ($LiPF_6$-based electrolyte). (d) Rate performance of PGDBs (LiTFSI-based electrolyte). (e) Cycle performance of PGDBs ($LiPF_6$-based electrolyte) at a current of 1.0 A g^{-1}.

curves gradually increasing (Fig. S3b). Electrochemical impedance spectroscopy (EIS) was used to gain insight into the activation evolution. As shown in Figs. S3c and 3d, the overall resistance decreased during activation and tended toward a steady state in the subsequent process. From these results it can be deduced that both the capacity and the reaction kinetics underwent an activation process during initial cycling.

The most outstanding feature of the PGDBs was their ultrahigh capacity retention under ultrafast charging conditions. After the activation period, the PGDBs showed stable reversible capacities of 120, 118, and 117 mAh g^{-1} at current levels of 0.5, 1.0, and 2.0 A g^{-1}, respectively. Unexpectedly, there was no significant capacity drop when the current increased to 5, 10, and 20 A g^{-1} (Fig. 1c). Even at a higher mass loading (10 mg_{PPy} cm^{-2}) and ultrafast charging currents of 10 and 20 A g^{-1}, the PGDBs still rendered a capacity of 111 and 105 mAh g^{-1}, corresponding to 92% and 87% of the initial specific capacity (Fig. 1c). Neither serious electrochemical polarization nor voltage drop were observed, even under fast discharge/charge conditions (Figs. S2b and S4a). PGDBs with a mass loading of 5 mg_{PPy} cm^{-2} achieved a high energy density of 372 Wh kg^{-1} at various power densities (Fig. S4b). Even at a high mass loading of 10 mg_{PPy} cm^{-2}, the energy density was 356, 344, and 325 Wh kg^{-1} at power densities of 15, 31, and 62 kW kg^{-1}, respectively (Fig. S4b).

Fig. 1e illustrates the long-term cycling performance of the PGDBs at a current of 1.0 A g^{-1}. After the activation period and on the way to stability, the PGDBs delivered a discharge capacity of 122 mAh g^{-1} and a cycle retention of 87% up to 3000 cycles, corresponding to a capacity decay of 0.0043% per cycle. Even with high active material loading (10 mg cm^{-2}), the cycling stability was excellent (91% capacity retention at 2.0 A g^{-1} over 2000 cycles) (Fig. S4c). Notably, the unprecedented high rate capability presented here changes our understanding of anion-insertion electrodes and their typically sluggish kinetic behavior with bulky anions, especially considering the electrode was fabricated without special techniques such as compositing with conductive carbon materials (e.g., nanotubes or graphene) and did not require high active material loading [28,29].

To determine how anions influenced the electrochemical behavior, we used lithium bis(trifluoromethane)sulfonimide (LiTFSI), a bulky anion (Figs. S5 and S6). The overall electrochemical behavior was like that of a $LiPF_6$-based electrolyte, apart from a lower average discharge potential and specific capacity (Fig. 1a and b). When the anion was replaced with $TFSI^-$, the rate capability and cycling stability remained excellent, suggesting anion size did not have a significant impact on performance and thus demonstrating the wide applicability of PPy as a high-rate DIB cathode (Fig. S5b). With the LiTFSI system, a lower capacity of 106 mAh g^{-1} was obtained, whereas the capacity with $LiPF_6$ was 120 mAh g^{-1} (Fig. 1a). This was probably because the insertion/extraction of bulky anions occupied more space around the charged polymer chains, thus limiting the number of accessible counteranions and the doping depth.

It is a well-established working principle that OEMs are adaptable to various charge carriers, implying the same electrode material is generally applicable with different counterions. To validate this assumption, we tested the electrochemical performance of PPy in a potassium organic battery (PPy||K). The battery delivered a capacity of 110 mAh g^{-1} and exhibited excellent reversibility without any obvious voltage hysteresis from 50 to 2000 mA g^{-1} (Figs. S8a and S8c). Impressively, the PPy||K battery also exhibited superior rate capability (Fig. S8b). From 100 to 4000 mA g^{-1}, its capacity did not decay as the rate increased. Even at a high current of 8.0 A g^{-1}, the capacity remained at 116 mAh g^{-1}. The battery also exhibited a remarkably long life, retaining 78% of the initial capacity after 1700 cycles at 1.0 A g^{-1} (Fig. S8d).

Based on the above investigations, we determined that the intrinsic fast reaction kinetics played a crucial role in achieving high rate performance. To gain further insight, we analyzed the relevant reaction kinetics. Fig. 2a shows the CV curves at various scan rates. As the sweep rate increased from 0.1 to 2 mV s^{-1}, the cathodic and anodic peaks at 2.74 and 2.60 V shifted to 3.64 and 2.31 V, respectively, and the separation of the anodic and cathodic peak potentials (ΔE_p) changed from 0.13 to 0.27 V, implying fast reaction kinetics. The ultrafast kinetic response appeared to be related to the capacitive-controlled reaction processes [30]. By establishing the correlation between response current (i) and sweep rate (v), we could analyze the capacitive- and diffusion-controlled processes. As shown in Fig. 2b, the calculated b-value approached 1.0 for both the anodic peak (1.013) and the cathodic peak (1.049). Clearly, fast near-surface activities made substantial contributions to the total current. Fig. 2c shows a typical CV curve at 2.0 mV s^{-1}, where the plotted capacitive current can be integrated into the pale-yellow area and is differentiated from the total current. The ratios of stored charge contributed by the capacitive mechanism at various scan rates are all close to 100%, indicating that the fast kinetics occurring on the surface of PPy were related to the pseudocapacitive effect (Fig. 2d).

It is generally agreed that the rapid mass transport of counterions is indispensable for a fast-charging battery. To investigate the anion diffusion dynamics, we used the GITT method to estimate the diffusion coefficient (D) of PF_6^- in PPy (Fig. 2e, Fig. S9). Fig. 2f shows the diffusion coefficient as a function of potential, with its average value ranging from 10^{-11} to 10^{-9} cm^2 s^{-1}. In the charge process, the D values were stable in the potential region from 2.54 to 3.63 V (~10^{-9} cm^2 s^{-1}) before reaching a minimum when close to the upper cutoff voltage. In the discharge process, the D values ranged from 3.6 × 10^{-9} to 1.6 × 10^{-10} cm^2 s^{-1} before the voltage dropped below 2.45 V. This rapid anion diffusion occurred even when bulky $TFSI^-$ anions were employed (Figs. S10 and S11).

To achieve high rate performance, two essential factors are rapid reaction kinetics at active sites and fast charge transport (i.e., electronic or ionic conduction). Electronic or ionic transport should be rapid enough to respond to the fast charge transfer reaction. In the charging

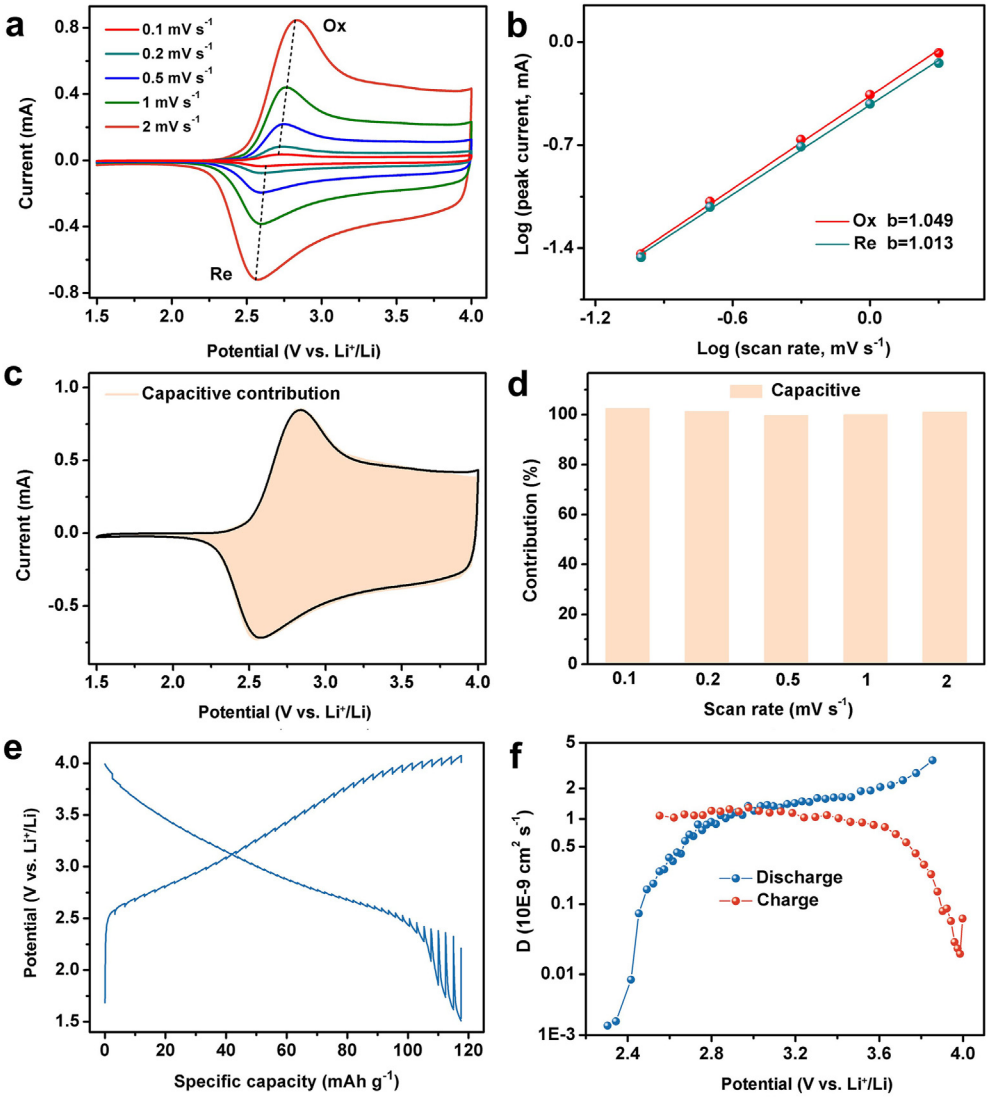

Fig. 2. Electrochemical performance of PPy||Li with 1.0 M $LiPF_6$ EC/DMC as electrolyte. (a) CV curves at various scan rates. (b) Power law dependence of measured current on scan rate at corresponding peak potentials. (c) Capacitive contribution at 2.0 mV s^{-1}. The peach area shows the contribution to capacitive charge storage. (d) Contribution ratios of capacitive charge storage at different scan rates. (e) Full charge/discharge GITT curve. (f) Diffusion coefficient (D) estimated with GITT methods.

process, electrons are extracted from the π-conjugated polymer chain of PPy. Afterwards, the positive charge left on the chain is neutralized by anions from the electrolyte (Fig. 3a, Scheme S2). The charge transfer rate of the redox-active polymers exerts a decisive effect on the kinetic performance. To maintain charge neutrality, this process should be conjugated with the timely diffusion of electrolyte counterions. With the conjugated polymers, charge transfer is achieved by carriers hopping between redox centers, accompanied by the diffusion of counterions. The charge propagation behavior can be described using a heterogeneous reaction rate constant (k^0) [31,32], which can be calculated using the Laviron method (Fig. 3b, Fig. S7a). Due to efficient charge transfer kinetics and facilitated ionic mobility, the k^0 value (7.5×10^{-3} cm s^{-1}) is high, indicating the rapid achievement of reaction equilibrium.

As is known, the "ion transfer" barrier at the electrolyte/electrode interface originates from two different processes: (1) desolvation of Li^+ before insertion into the host and (2) the subsequent migration of bare Li^+ through the interface [33]. The stripping of the solvation sheath from Li^+ is assumed to be the rate-determining step at the electrolyte/electrode interface [34]. Due to the small ionic radius, there is a strong Coulombic attraction between Li^+ and the solvent molecules. Hence, metal cation desolvation is treated as the most energy-consuming step in the cation-insertion mechanism [35]. Unlike with the cation (Li^+), the solvation effect on the bulk anions (PF_6^- and $TFSI^-$) is weak, due to their large anionic radii and low electric charge density. In this situation, anion transport from electrolyte to host structure may be the most energy-consuming process.

It is generally known that the reductive decomposition potential of most carbonate-based electrolytes starts below 1.0 V versus Li^+/Li. Oxidation decomposition is unlikely to occur at potentials below 4.0 V. It is therefore reasonable to suppose that the battery was operating in a safe electrochemical window. In a sense, PPy could be considered an "interface-free" electrode material that accommodates anions (PF_6^- or $TFSI^-$), making it possible to study the anion transfer barrier at the electrolyte/PPy junction. The absence of a passivation layer means migration across the interface can be ignored. We obtained temperature-dependent impedance spectra to analyze this thermally activated process and evaluated the charge transfer activation energies ($E_{a,ct}$), based on Arrhenius theory. Fig. 3c shows selected impedance spectra of PPy||Li at different temperatures. In the PF_6^- system, the activation energy for the charge-transfer component was around 50.15 kJ mol^{-1}, while bulky $TFSI^-$ overcame a higher energy barrier (62.12 kJ mol^{-1}), indicating the superiority of size when anion insertion happens (Figs. S7b and S12).

In the anion-insertion mechanism, the oxidation of PPy removed electrons from the π-conjugated chain, and PF_6^- counterions from the electrolyte moved towards the electrode, balancing the positively charged polymer chain (Fig. 4a). We used X-ray photoelectron spectroscopy (XPS) to probe the PF_6^- anion reaction process (Figs. 4b and c, Fig. S13). In the fully charged state, the appearance of P 2p and F 1s signals implied that the PF_6^- anions were incorporated into the PPy cathode. When discharged to 1.4 V, neither of those peaks were observable, indicating the release of the PF_6^- back to the electrolyte during the reduction process.

A polymer's microstructure exerts fundamental effects on the electrode's reaction kinetics [36–38]. It has been found that large aromatic dopants such as *p*TSNa affect the arrangement of polymer chains, engaging with the aromatic pyrrole ring through π–π interactions that lead to laminar growth [39,40]. The electron-rich *p*TS^- groups act as electron tanks, which can exchange electrons with the conjugated backbone of PPy and undoubtedly enhance interchain interactions. Increased conjugation length is a direct consequence of the π–π interaction between the polymer backbone and the dopant *p*TS^-, wherein the *p*TS^- helps form conducting domains of large magnitude [41,42]. It can also impact the conduction channel inside the polymer matrix through the formation of bipolaronic and polaronic species for effective charge

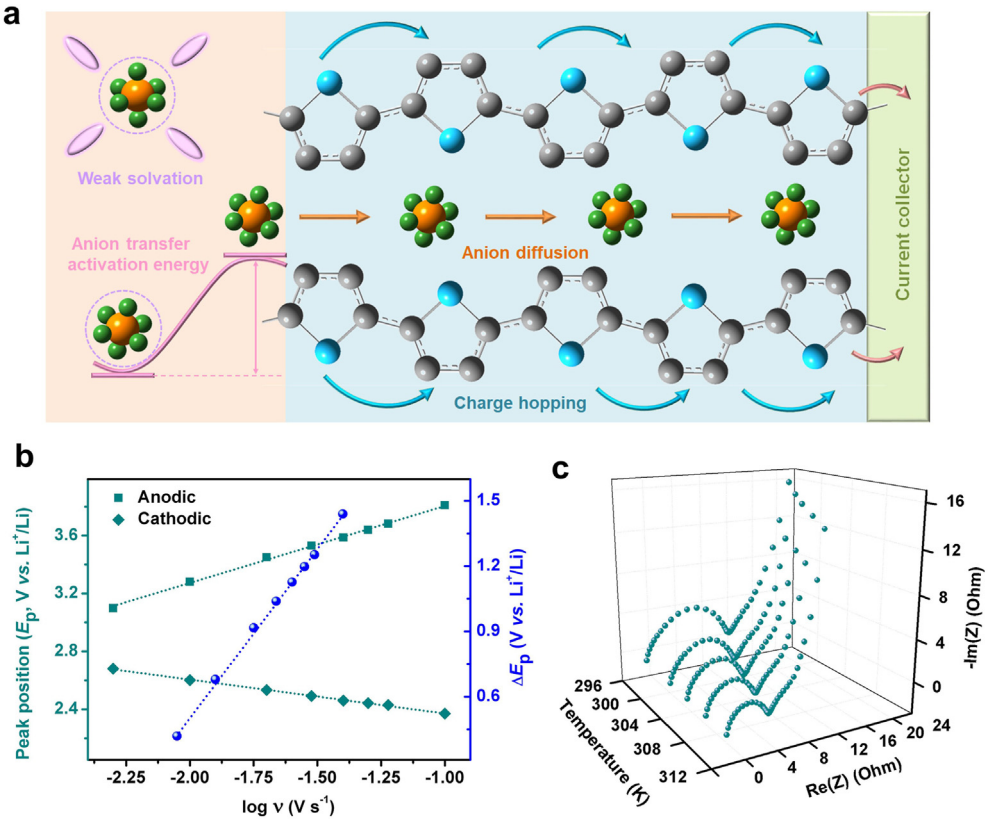

Fig. 3. (a) Schematic illustration of the reaction kinetics of PPy. (b) Variations in anodic and cathodic peak positions (E_p), and ΔE_p as a function of the scan rate. (c) Temperature-dependent EIS analysis of PPy||Li cell with $LiPF_6$-based electrolyte.

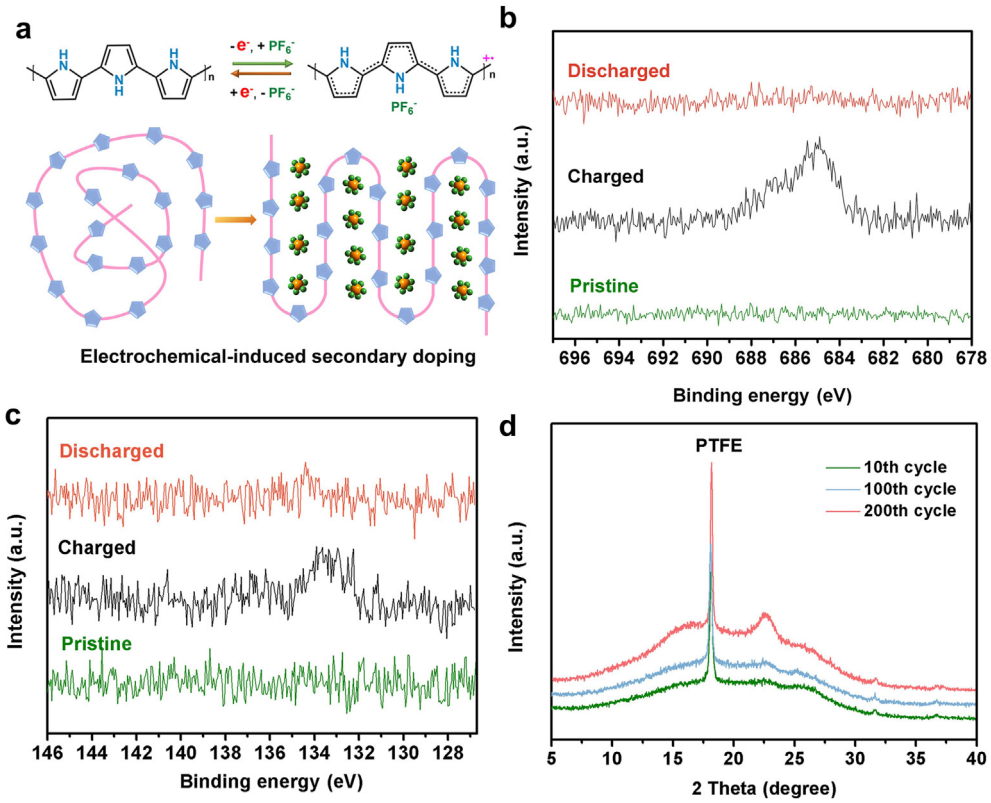

Fig. 4. (a) Schematic illustration of the reaction mechanism of PPy during PF_6^- storage. (b) XPS spectra of F 1s region. (c) XPS spectra of P 2p region. (d) XRD pattern of PPy electrode at different cycles.

transfer [43]. Due to the anions stored between the chain layers of polymers, an ordered arrangement of the polymer matrix balances the electrostatic forces between the positively charged segments of PPy chains and the negatively charged dopant ions distributed across the interchain space. The electrostatic attraction between the positively charged segments of PPy chains and dopant anions can effectively prevent the electrode from cracking or being pulverized (Figs. S14–S16). In another sense, the continual insertion/extraction of counteranions with the polymer electrode material can be regarded as secondary doping induced by the electrochemical conditions [44,45]. Just as inorganic electrode materials undergo structural reconstruction or phase transformation in an electrochemical environment, a similar phenomenon can be observed in organic materials [46,47].

In the present work, we studied the structure of PPy crystalline regions after repeated charge/discharge cycles with PF_6^- as the counterion. We propose that the continual electrochemical stimulation improved the crystallinity of PPy or the packing of its polymer chains, which was beneficial for effective charge transfer among the intrachains or interchains of PPy. As shown in Fig. 4d, better aggregation of the polymer chains was apparent after the activation process finished.

The ordered packing in conjugated polymers originates from a coplanar stacked structure that exhibits strong π-orbital overlap. Conjugated polymer chains are inclined to form stacked aggregates with a relative degree of crystallinity, which can be detected by the width and strength of their XRD scattering peaks. Fig. 4d shows the XRD pattern for PPy, which displays two obvious broad peaks at approximately $2\theta = 15.4^\circ$ and 22.5°. The diffraction peak at 15.4° is generally assigned to the distance between pyrrolic planes with interfaced aromatic rings. The peak situated at 22.4° is ascribed to the interplanar spacing of pyrrole rings. Clearly, the polymer could be ordered in various crystallographic directions. This assumption was also supported by the micro-level structure of cycled PPy, in which crystalline islands with ordered orientations were discerned (Fig. S15). Hence, the continual doping/dedoping process improved the crystallinity of PPy or the packing of its polymer chains, which exhibiting a self-adapting capability for the intercalated anions.

We know that π–π stacking is a relatively strong interchain interaction where unpaired π electrons are shared by overlapping with the adjacent conjugated ring [45]. Tuning the degree of crystallinity to improve the packing structure as well as the orbital shape, orientation, and symmetry can facilitate charge transport in aggregates. It is believed that conjugated chains closely stacked along a specific direction result in longer conjugated chain segments, yielding better electrical conductivity. This assumption could also explain the sluggish activation process during cycling, in which the electrochemical resistance decreased as the cycling depth increased.

In the quest for electrochemical energy storage devices with both high energy density and power density, the line between electrochemical capacitors and batteries is becoming blurred [48–50]. There is now an accepted trend toward integrating the two devices, especially for redox electrode materials with pseudocapacitive activity [51]. To some extent, the DIBs presented here can also be regarded as dual-ion hybrid electrochemical devices. Unlike common electrical double-layer capacitors, this hybrid energy storage device is constituted by an anion host pseudocapacitive cathode and a Li^+ intercalated graphite anode. Combining the merits of capacitors and batteries yields a hybrid electrochemical device with simultaneously better energy and power densities (Fig. 5).

3. Conclusion

In summary, we have demonstrated that PPy can be used as an ultrafast, stable organic cathode for DIBs. The distinctive operating mechanism afforded PGDBs a reversible capacity of 125 mAh g^{-1} at a median discharge voltage of 3.1 V, together with an outstanding lifespan across 3000 cycles (83% capacity retention). With a higher mass loading (10 mg_{PPy} cm^{-2}) and under ultrafast charging currents of 10 and 20 A

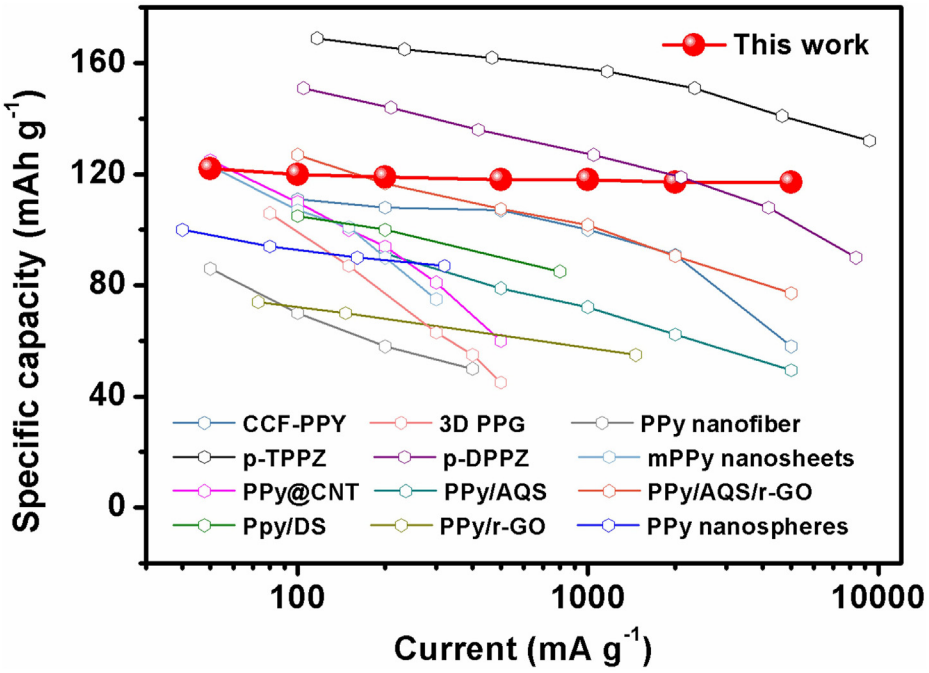

Fig. 5. Rate performance compared with other reported organic cathodes (CCF–PPY [52], 3D PPG [53], PPy nanofiber [54], *p*-DPPZ and *p*-TPPZ [55], mPPy nanosheets [56], PPy@CNT [57], PPy/AQS/r-GO and PPy/AQS [58], Ppy/DS [59], PPy/r-GO [60], and PPy nanospheres [61]).

g^{-1}, PGDBs still delivered a reversible capacity of 111 and 105 mAh g^{-1}, corresponding to 92% and 87% retention of the initial capacity. Apart from in a $LiPF_6$-based electrolyte, high rate performance was also observed in a LiTFSI system and even in a PPy||K battery. The intrinsic fast redox kinetics, coupled with a capacitance-dominated mechanism, explain the outstanding rate capability. We postulate that electrochemically induced secondary doping improved the ordered aggregation of the polymer chains, thereby having a profound impact on anion diffusion and electrical conductivity. The findings presented here not only further consolidate the family of high-rate OEMs but also provide rich mechanistic insights into intrinsic factors for further exploring advanced energy storage devices.

Declaration of competing interest

The authors declare that they have no known competing financial interests or personal relationships that could have appeared to influence the work reported in this paper.

Acknowledgments

This work was financially supported by National Key R&D Program of China (2017YFA0206700), National Natural Science Foundation of China (21725103), K. C. Wong Education Foundation (GJTD-2018-09). Jilin Province Science and Technology Development Plan Funding Project (20200201079JC), Jilin Province Capital Construction Funds Project (2020C026-1).

Appendix A. Supplementary data

Supplementary data to this article can be found online at https://doi.org/10.1016/j.esci.2021.11.003.

References

[1] J. Liu, J. Wang, C. Xu, H. Jiang, C. Li, L. Zhang, J. Lin, Z.X. Shen, Advanced energy storage devices: basic principles, analytical methods, and rational materials design, Adv. Sci. 5 (2018) 1700322.

[2] L. Zhang, H. Wang, X. Zhang, Y. Tang, A review of emerging dual-ion batteries: fundamentals and recent advances, Adv. Funct. Mater. 31 (2021) 2010958.

[3] F. Wu, J. Maier, Y. Yu, Guidelines and trends for next-generation rechargeable lithium and lithium-ion batteries, Chem. Soc. Rev. 49 (2020) 1569–1614.

[4] Y. Cao, M. Li, J. Lu, J. Liu, K. Amine, Bridging the academic and industrial metrics for next-generation practical batteries, Nat. Nanotechnol. 14 (2019) 200–207.

[5] E. Fan, L. Li, Z. Wang, J. Lin, Y. Huang, Y. Yao, R. Chen, F. Wu, Sustainable recycling technology for Li-ion batteries and beyond: challenges and future prospects, Chem. Rev. 120 (2020) 7020–7063.

[6] C. Jiang, Y. Fang, J. Lang, Y. Tang, Integrated configuration design for ultrafast rechargeable dual-ion battery, Adv. Energy Mater. 7 (2017) 1700913.

[7] X. Zhang, Y. Tang, F. Zhang, C.-S. Lee, A novel aluminum–graphite dual-ion battery, Adv. Energy Mater. 6 (2016) 1502588.

[8] T. Placke, A. Heckmann, R. Schmuch, P. Meister, K. Beltrop, M. Winter, Perspective on performance, cost, and technical challenges for practical dual-ion batteries, Joule 2 (12) (2018) 2528–2550.

[9] L. Fan, Q. Liu, S. Chen, K. Lin, Z. Xu, B. Lu, Potassium-based dual ion battery with dual-graphite electrode, Small 13 (30) (2017) 1701011.

[10] X. Tong, F. Zhang, B. Ji, M. Sheng, Y. Tang, Carbon-coated porous aluminum foil anode for high-rate, long-term cycling stability, and high energy density dual-ion batteries, Adv. Mater. 28 (2016) 9979–9985.

[11] T. Placke, O. Fromm, S.F. Lux, P. Bieker, S. Rothermel, H.-W. Meyer, S. Passerini, M. Winter, Reversible intercalation of bis(trifluoromethanesulfonyl)imide anions from an ionic liquid electrolyte into graphite for high performance dual-ion cells, J. Electrochem. Soc. 159 (2012) A1755–A1765.

[12] S. Rothermel, P. Meister, G. Schmuelling, O. Fromm, H.-W. Meyer, S. Nowak, M. Winter, T. Placke, Dual-graphite cells based on the reversible intercalation of bis(trifluoromethanesulfonyl)imide anions from an ionic liquid electrolyte, Energy Environ. Sci. 7 (2014) 3412–3423.

[13] L. Fan, Q. Liu, Z. Xu, B. Lu, An organic cathode for potassium dual-ion full battery, ACS Energy Lett 2 (7) (2017) 1614–1620.

[14] L. Fan, R. Ma, J. Wang, H. Yang, B. Lu, An ultrafast and highly stable potassium–organic battery, Adv. Mater. 30 (2018) 1805486.

[15] I.A. Rodríguez-Pérez, C. Bommier, D.D. Fuller, D.P. Leonard, A.G. Williams, X. Ji, Toward higher capacities of hydrocarbon cathodes in dual-ion batteries, ACS Appl. Mater. Interfaces 10 (2018) 43311–43315.

[16] I.A. Rodríguez-Pérez, X. Ji, Anion hosting cathodes in dual-ion batteries, ACS Energy Lett 2 (8) (2017) 1762–1770.

[17] P. Poizot, J. Gaubicher, S. Renault, L. Dubois, Y. Liang, Y. Yao, Opportunities and challenges for organic electrodes in electrochemical energy storage, Chem. Rev. 120 (2020) 6490–6557.

[18] H. Peng, Q. Yu, S. Wang, J. Kim, A.E. Rowan, A.K. Nanjundan, Y. Yamauchi, J. Yu, Molecular design strategies for electrochemical behavior of aromatic carbonyl compounds in organic and aqueous electrolytes, Adv. Sci. 6 (2019) 1900431.

[19] M. Tang, S. Zhu, Z. Liu, C. Jiang, Y. Wu, H. Li, B. Wang, E. Wang, J. Ma, C. Wang, Tailoring π-conjugated systems: from π-π Stacking to high-rate-performance organic cathodes, Inside Chem. 4 (11) (2018) 2600–2614.

[20] Y. Chen, C. Wang, Designing high performance organic batteries, Accounts Chem. Res. 53 (2020) 2636–2647.

[21] Z. Zhu, J. Chen, Review—advanced carbon-supported organic electrode materials for lithium (sodium)-ion batteries, J. Electrochem. Soc. 162 (2015) A2393–A2405.
[22] H. Li, Practical evaluation of Li-ion batteries, Joule 3 (4) (2019) 911–914.
[23] H. Chen, H. Xu, S. Wang, T. Huang, J. Xi, S. Cai, F. Guo, Z. Xu, W. Gao, C. Gao, Ultrafast all-climate aluminum-graphene battery with quarter-million cycle life, Sci. Adv. 3 (2017) eaao7233.
[24] T. Janoschka, M.D. Hager, U.S. Schubert, Powering up the future: radical polymers for battery applications, Adv. Mater. 24 (2012) 6397–6409.
[25] Y. Liang, Y. Yao, Positioning organic electrode materials in the battery landscape, Joule 2 (9) (2018) 1690–1706.
[26] Z. Song, H. Zhou, Towards sustainable and versatile energy storage devices: an overview of organic electrode materials, Energy Environ. Sci. 6 (2013) 2280–2301.
[27] L. Qie, L.-X. Yuan, W.-X. Zhang, W.-M. Chen, Y.-H. Huang, Revisit of polypyrrole as cathode material for lithium-ion battery, J. Electrochem. Soc. 159 (2012) A1624–A1629.
[28] T. Fukutsuka, F. Yamane, K. Miyazaki, T. Abe, Electrochemical intercalation of bis(fluorosulfonyl)amide anion into graphite, J. Electrochem. Soc. 163 (2016) A499–A503.
[29] A. Heckmann, P. Meister, L.-Y. Kuo, M. Winter, P. Kaghazchi, T. Placke, A route towards understanding the kinetic processes of bis(trifluoromethanesulfonyl) imide anion intercalation into graphite for dual-ion batteries, Electrochim. Acta 284 (2018) 669–680.
[30] J. Tian, D. Cao, X. Zhou, J. Hu, M. Huang, C. Li, High-capacity Mg–organic batteries based on nanostructured rhodizonate salts activated by Mg–Li dual-salt electrolyte, ACS Nano 12 (4) (2018) 3424–3435.
[31] N. Patil, A. Mavrandonakis, C. Jérôme, C. Detrembleur, J. Palma, R. Marcilla, Polymers bearing catechol pendants as universal hosts for aqueous rechargeable H^+, Li-Ion, and post-Li-ion (mono-, di-, and trivalent) batteries, ACS Appl. Energy Mater. 2 (2019) 3035–3041.
[32] N. Patil, A. Aqil, F. Ouhib, S. Admassie, O. Inganäs, C. Jérôme, C. Detrembleur, Bioinspired redox-active catechol-bearing polymers as ultrarobust organic cathodes for lithium storage, Adv. Mater. 29 (2017) 1703373.
[33] K. Xu, A. von Cresce, U. Lee, Differentiating contributions to "Ion transfer" barrier from interphasial resistance and Li^+ desolvation at electrolyte/graphite interface, Langmuir 26 (13) (2010) 11538–11543.
[34] K. Xu, A. von Cresce, Interfacing electrolytes with electrodes in Li ion batteries, J. Mater. Chem. 21 (2011) 9849–9864.
[35] M. Li, C. Wang, Z. Chen, K. Xu, J. Lu, New concepts in electrolytes, Chem. Rev. 120 (14) (2020) 6783–6819.
[36] S. Iwasa, T. Nishi, S. Nakamura, Enhancement of rapid charging capability of organic radical battery using ethylene carbonate-based electrolyte containing LiFSI, J. Power Sources 402 (2018) 157–162.
[37] L. Zhang, H. Wang, X. Zhang, Y. Tang, A review of emerging dual-ion batteries: fundamentals and recent advances, Adv. Funct. Mater. 31 (2021) 2010958.
[38] J.J. Shea, C. Luo, Organic electrode materials for metal ion batteries, ACS Appl. Mater. Interfaces 12 (2020) 5361–5380.
[39] A. Kumar, R.K. Singh, K. Agarwal, H.K. Singh, P. Srivastava, R. Singh, Effect of p-toluenesulfonate on inhibition of overoxidation of polypyrrole, J. Appl. Polym. Sci. 130 (2013) 434–442.
[40] M. Omastova, M. Trchova, J. Kovarova, J. Stejskal, Synthesis and structural study of polypyrroles prepared in the presence of surfactants, Synthetic Met 138 (2003) 447–455.
[41] L.-X. Wang, X.-G. Li, Y.-L. Yang, Preparation, properties and applications of polypyrroles, React. Funct. Polym. 47 (2001) 125–139.
[42] Y. Kudoh, Properties of polypyrrole prepared by chemical polymerization using aqueous solution containing $Fe_2(SO_4)_3$ and anionic surfactant, Synthetic Met 79 (1996) 17–22.
[43] A. Kumar, R.K. Singh, H.K. Singh, P. Srivastava, R. Singh, Enhanced capacitance and stability of p-toluenesulfonate doped polypyrrole/carbon composite for electrode application in electrochemical capacitors, J. Power Sources 246 (2014) 800–807.
[44] K. Kanamura, Y. Kawai, S. Yonezawa, Z. Takehara, Diffusion behavior of anions in polyaniline during electrochemical undoping. 2. Effect of the preparation conditions of polyaniline on the diffusion coefficient of BF_4, J. Phys. Chem. 98 (1994) 2174–2179.
[45] T.y.V. Vernitskaya, O.N. Efimov, Polypyrrole: a conducting polymer; its synthesis, properties and applications, Russ. Chem. Rev. 66 (1997) 443–457.
[46] G. Dai, Y. Liu, Z. Niu, P. He, Y. Zhao, X. Zhang, H. Zhou, The design of quaternary nitrogen redox center for high-performance organic battery materials, Matter 1 (2019) 945–958.
[47] Z. Niu, H. Wu, L. Liu, G. Dai, S. Xiong, Y. Zhao, X. Zhang, Chain rigidity modifification to promote the electrochemical performance of polymeric battery electrode materials, J. Mater. Chem. 7 (2019) 10581–10588.
[48] W.H. Li, H.J. Liang, X.K. Hou, Z.Y. Gu, X.X. Zhao, J.Z. Guo, X. Yang, X.L. Wu, Feasible engineering of cathode electrolyte interphase enables the profoundly improved electrochemical properties in dual-ion battery, J. Energy Chem. 50 (2020) 416–423.
[49] X. Hou, W. Lia, Y. Wang, S. Li, Y. Meng, H. Yu, B. Chen, X. Wu, Sodium-based dual-ion batteries via coupling high-capacity selenium/graphene anode with high-voltage graphite cathode, Chin. Chem. Lett. 31 (2020) 2314–2318.
[50] W.H. Li, Q.L. Ning, X.T. Xi, B.H. Hou, J.Z. Guo, Y. Yang, B. Chen, X.L. Wu, Highly improved cycling stability of anion de-/intercalation in the graphite cathode for dual-ion batteries, Adv. Mater. 31 (2019) 1804766.
[51] S. Fleischmann, J.B. Mitchell, R. Wang, C. Zhan, D.E. Jiang, V. Presser, V. Augustyn, Pseudocapacitance: from fundamental understanding to high power energy storage materials, Chem. Rev. 120 (14) (2020) 6738–6782.
[52] Z. Wang, C. Xu, P. Tammela, P. Zhang, K. Edstrçm, T. Gustafsson, M. Strømme, L. Nyholm, Conducting polymer paper-based cathodes for high-areal-capacity lithium–organic batteries, Energy Technol. 3 (2015) 563–569.
[53] S. Liu, F. Wang, R. Dong, T. Zhang, J. Zhang, Z. Zheng, Y. Mai, X. Feng, Soft-template construction of 3D macroporous polypyrrole scaffolds, Small 13 (2017) 1604099.
[54] X. Li, D. Fang, Y. Cao, Z. Luo, M. Jiang, W. Xu, C. Xiong, Template-sacrificed synthesis of polypyrrole nanofibers for lithium battery, J. Mater. Sci. 51 (2016) 9526–9533.
[55] S. Xu, H. Dai, S. Zhu, Y. Wu, M. Sun, Y. Chen, K. Fan, C. Zhang, C. Wang, W. Hu, A branched dihydrophenazine-based polymer as a cathode material to achieve dual-ion batteries with high energy and power density, eScience (2021), https://doi.org/10.1016/j.esci.2021.08.002.
[56] S. Liu, F. Wang, R. Dong, T. Zhang, J. Zhang, X. Zhuang, Y. Mai, X. Feng, Dual-template synthesis of 2D mesoporous polypyrrole nanosheets with controlled pore size, Adv. Mater. 28 (2016) 8365–8370.
[57] J. Duan, D. Zou, J. Li, J. Weng, Y. Liu, S. Gong, A. Li, P. Zhou, One-dimensional PPy@CNT based on reversible anions doping/dedoping as a novel high-performance cathode for potassium based double ion batteries, Electrochim. Acta 376 (2021) 138047.
[58] Y. Yang, K. He, P. Yan, D. Wang, X. Wu, X. Zhao, Z. Huang, C. Zhang, D. He, Enhanced capacity of polypyrrole/anthraquinone sulfonate/graphene composite as cathode in lithium batteries, Electrochim. Acta 138 (2014) 481–485.
[59] M. Zhou, Y. Xiong, Y. Cao, X. Ai, Electroactive organic anion-doped polypyrrole as a low cost and renewable cathode for sodium-ion batteries, J. Polym. Sci., Part B: Polym. Phys. 51 (2013) 114–118.
[60] Y. Yang, C. Wang, B. Yue, S. Gambhir, C.O. Too, G.G. Wallace, Electrochemically synthesized polypyrrole/graphene composite film for lithium batteries, Adv. Energy Mater. 2 (2012) 266–272.
[61] D. Su, J. Zhang, S. Dou, G. Wang, Polypyrrole hollow nanospheres: stable cathode materials for sodium-ion batteries, Chem. Commun. 51 (2015) 16092.